Beam Shaping with Tip-Tilt Varifocal Mirror for Optical Wireless Communication

Corey Pollock,[1] Jessica Morrison,[2] Matthias Imboden,[3] Thomas D.C. Little,[2] and D.J. Bishop[2,3,4,5]

[1]*Department of Mechanical Engineering, Boston University, Boston, Massachusets, USA*
[2]*Department of Electrical and Computer Engineering, Boston University, Boston, Massachusets, USA*
[3]*'Ecole Polytechnique Fédérale de Lausanne (EPFL), Neuchâtel, Switzerland*
[4]*Division of Material Science and Engineering, Boston University, Boston, Massachusets, USA*
[5]*Department of Physics, Boston University, Boston, Massachusets, USA*
[*]*cpollock@bu.edu*

Abstract: MEMS mirrors are currently used in many applications to steer beams of light. An area of continued research is developing mirrors with varifocal capability that allows the beam to be shaped and focused. In this work, we study the varifocal capability of a 400 μm diameter, thermally actuated MEMS mirror with a ± 40° tip-tilt angle and a radius of curvature between -.48 mm to 20.5 mm. Light is delivered to the mirror via a single mode optical fiber, similar to an optical wireless communication architecture. The performance of the mirror is characterized with regards to (1) the profile of the reflected beam as the mirror deforms and (2) the mirror's ability to significantly improve the bit error rate of an optical communication system by focusing the light onto a detector.

OCIS codes: (230.3990) Micro-optical devices; (230.4040) Mirrors; (220.1080) Active or adaptive optics; (060.2605) Free-space optical communication; (060.2390) Fiber optics, infrared.

References and links

1. V. Milanović, A. Kasturi, V. Hachtel, and M. Technologies, "High Brightness MEMS Mirror Based Head-Up Display (HUD) Modules with Wireless Data Streaming Capability," (2015).
2. J. Reitterer, F. Fidler, G. Schmid, T. Riel, C. Hambeck, F. Saint Julien-Wallsee, W. Leeb, and U. Schmid, "Design and evaluation of a large-scale autostereoscopic multi-view laser display for outdoor applications," Optics Express **22**, 27063 (2014).
3. M. Strathman, Y. Liu, X. Li, and L. Y. Lin, "Dynamic focus-tracking MEMS scanning micromirror with low actuation voltages for endoscopic imaging," Optics express **21**, 23934–23941 (2013).
4. L. Li, R. Li, W. Lubeigt, and D. Uttamchandani, "Design, simulation, and characterization of a bimorph varifocal micromirror and its application in an optical imaging system," Journal of Microelectromechanical Systems **22**, 285–294 (2013).
5. P. Brandl, S. Member, S. Schidl, A. Polzer, W. Gaberl, H. Zimmermann, and S. Member, "Optical Wireless Communication With Adaptive Focus and MEMS-Based Beam Steering," IEEE Photonics Technology Letters **25**, 1428–1431 (2013).
6. T. Sasaki and K. Hane, "Varifocal micromirror integrated with comb-drive scanner on silicon-on-insulator wafer," Journal of Microelectromechanical Systems **21**, 971–980 (2012).
7. R. Hokari and K. Hane, "Micro-mirror laser scanner combined with a varifocal mirror," Microsystem Technologies **18**, 475–480 (2012).
8. J. Morrison, M. Imboden, T. D. C. Little, and D. J. Bishop, "Electrothermally actuated tip-tilt-piston micromirror with integrated varifocal capability," Optics Express **23**, 9555–9566 (2015).
9. C. W. Oh, Z. Cao, E. Tangdiongga, and T. Koonen, "Free-space transmission with passive 2D beam steering for multi-gigabit-per-second per-beam indoor optical wireless networks," Optics Express **24**, 19211 (2016).
10. K. Wang, a. Nirmalathas, C. Lim, and E. Skafidas, "High-Speed Optical Wireless Communication System for Indoor Applications," Photonics Technology Letters, IEEE **23**, 519–521 (2011).
11. H. Zappe, "Fundamentals of Micro-Optics," in "Fundamentals of Micro-Optics," (Cambridge University Press, 2010), chap. 8, pp. 265–319, 1st ed.
12. "Focal Length," https://www.rp-photonics.com/focal_length.html.
13. M. T.-K. Hou and R. Chen, "Effect of width on the stress-induced bending of micromachined bilayer cantilevers," Journal of Micromechanics and Microengineering **13**, 141–148 (2002).
14. L. Couch, "Digital and Analog Communication Systems," in "Digital and Analog Communication Systems," (Pearson, 2007), chap. 7, pp. 476–550, 7th ed.

1. Introduction

Microelectromechanical systems (MEMS) are used in a wide range of optical applications. These applications include laser displays [1, 2], imaging [3, 4], and communications [5] to name a few. Most of the current research and all commercially available MEMS scanners use flat mirrors. The setups typically include optics to shape the beam before reaching the mirror, and the mirror then directs the beam. These systems work well, however one of the limitations is that they have to work with a fixed focal length and/or beam size. An area of current research is developing mirrors which have the capability to change their focal length, and therefore also their beam size [6, 7]. We have developed a thermally actuated varifocal mirror, shown in Figure 1, that has a ± 40° tip-tilt range and also has a tunable radius of curvature (ROC) range from -.48 mm to 20.5 mm [8]. For example, using the setup presented in this paper this allows a beam to be steered around a room at ± 40° optical while at the same time, the beam diameter can be less than 5 mm or greater than 50 mm when 0.5 m from the mirror. This paper focuses primarily on the varifocal aspect of the mirror and its applications.

One of the applications that will benefit from this mirror is optical wireless communications (OWC). Using a narrow beam will improve the signal to noise ratio (SNR) and lead to faster data transmissions. Because of the SNR considerations, OWC requires the ability to beam steer, or other methods for collimated beams of light. A device such as shown here is a practical, low cost way of doing this. There are, however, some situations when having a larger beam could be beneficial, such as when the transmitter is first locating the receiver, or when it's is tracking a receiver as it moves. Varifocal capability provides the opportunity to continuously optimize the beam for the specific scenario. One of the common architectures for OWC is with a fiber delivery system [9, 10]. This consists of a centralized communications system that can then deliver light to the transmitters via optical fibers compared to having each transmitter integrated with its own light source. The mirror's large tunable focal range allows it to be integrated into a fiberized system without additional optics, which could potentially lead to more compact designs and simpler manufacturing.

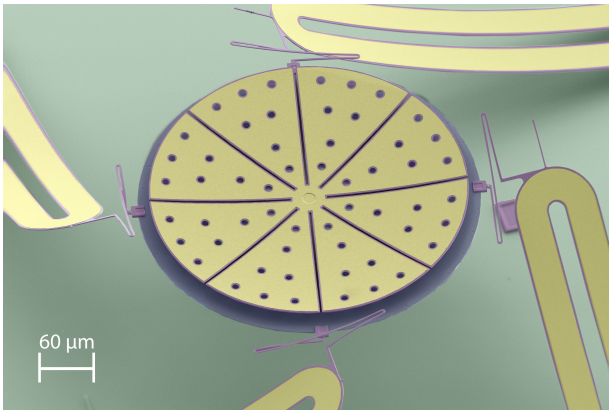

Fig. 1. False color SEM image of thermally actuated varifocal mirror connected to four thermal bimorphs via serpentine springs.

2. Setup/Method

The mirror used in this paper is fabricated using the MEMSCAPs multi-user PolyMUMPS process. It consists of three layers of polysilicon followed by a layer of gold. A residual tensile stress in the gold due to the evaporation process provides an initial curvature to the beam which results in an initial vertical displacement. Heating the bimorph causes it to bend downward due to the different magnitudes of thermal expansion of gold and polysilicon, producing vertical actuation. This concept can also be applied to a polysilicon-gold mirror. A circular mirror can be divided into sections that results in a spherically shaped mirror consisting of wedge shaped bimorphs. Heating the mirror via polysilicon heaters tunes the ROC and therefore the focal point of the mirror [8].

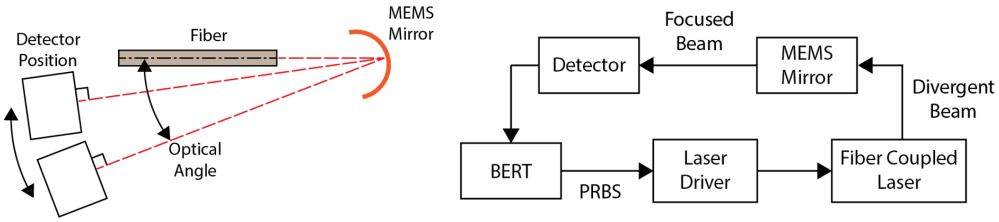

Fig. 2. (left) Illustration (not to scale) of test setup demonstrating that the detector is always normal to the reflected beam and is always the same distance from the mirror. (right) System schematic of the BERT system used for collecting BER data. A PXIe-6555 generates a PRBS which is used to control the laser driver and subsequently the fiber coupled laser. The light is focused using the MEMS mirror onto the detector whose signal is compared to the original PRBS signal in the PXIe-6555.

The setup presented in this paper emulates a fiberized system as shown in Figure 2. It used 1550 nm light coupled into a single mode optical fiber which outputs a Gaussian beam with a measured half angle divergence of 4.6°. The fiber was positioned with a relatively small initial angle to the mirror (1°-3°). To maximize the power from the mirror for subsequent experiments, the optimal distance between the fiber and the mirror was measured. The design of the mirror includes slots and holes which are important for the mirror's curvature and the fabrication process. This optimal fiber position that is dependent on the incident beam divergence angle and the specific mirror geometry (i.e. mirror radius, slots and holes). The measured data is compared to a Zemax simulation and a mathematical model of the mirror as shown in Figure 3. In this plot, the efficiency is defined as: $\eta = \frac{P_r}{P_t}$, where η is is efficiency, P_r is the power received and P_t is the power transmitted from the fiber. The simulated results agree with each other to within 3%. Although the measured optimal distance is within 6% of the simulations, the peak efficiency is only 83% of the simulations. In addition, as the fiber gets within 0.75 mm of the mirror, the efficiency doesn't improve as do the simulations. These discrepancies may result from two limitations/differences in the simulated models versus the experimental setup. First, in both the Zemax and mathematical models, the detectors are placed close enough to capture all the reflected light. Due to physical limitations of the test equipment, the detector was placed at a further distance and the beam was focused using the mirror, similar to how it would in later testing and applications. Second, simulations showed that misalignment between the fiber and the mirror has a larger effect on efficiency at distances closer than .75 mm. A misalignment of 30 μm is enough to eliminate the increase in efficiency under .75 mm but has little effect on the peak efficiency. This result is shown in Figure 3. Another possible explanation for this efficiency loss is by diffraction from the mirror. The Airy disk from a circular diffraction pattern contains 84%

of the total optical power, which would account for the discrepancy between the simulation and data [11]. Although the measured efficiency is significantly lower than the simulated result, an important finding from this study is that the absolute maximum efficiency of this mirror geometry is 80%. This could in principle be improved by removing the holes and reducing the size of the slots, although this may have unknown consequences on the mirrors curvature. This is important for future designs and studies. Based on these tests all future test setups placed the fiber 1.275 mm away from the mirror.

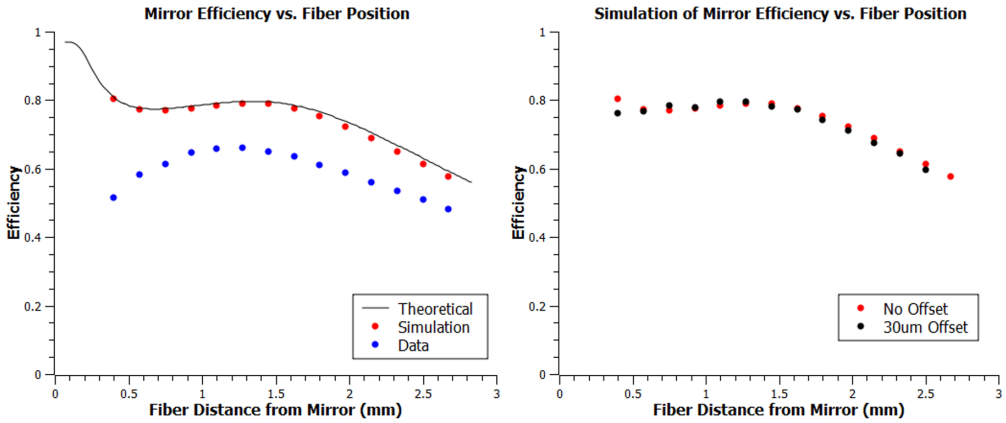

Fig. 3. (left) Plot of the optical efficiency vs. the distance between the end of the fiber and the mirror. Efficiency is defined as the ratio between the power reflected from the mirror and the power measured from the fiber. (right) Simulation showing the effect of a misalignment of 30 μu between the optical fiber and the mirror.

All testing of the mirror discussed here falls under two broad categories: characterizing the beam profile and characterizing the bit error rate (BER). For both sets of testing, the performance was characterized with respect to a) the power applied to the mirror (i.e. radius of mirror curvature), b) the optical angle of the beam, and c) the distance from the mirror to the detector. Unless otherwise stated, all testing used the setup illustrated in Figure 2. While characterizing the mirrors performance compared to angle, this setup maintained a fixed distance between the mirror and the detector. It also ensured that the light from the mirror arrived at an angle normal to the detector as shown in Figure 2. This allows the beam to be characterized with regards to the angle and shape of the reflected beam independently from the detector's position and orientation. A DataRay WinCamD-UHR camera with phosphor coating was used to collect the beam profile data. BER data was measured using an InGaAS variable-gain avalanche photodetector as part of the system illustrated in Figure 2. This consisted of a bit error rate tester (BERT) to generate and analyze a 20 bit pseudorandom binary sequence (PRBS) at 100 Mbps, a laser driver board, and the aforementioned detector. The peak optical output of the optical fiber was approximately 1 mW. In most cases during communication testing, this led to an error free connection (BER $< 10^{-9}$). To better characterize the performance of the mirror, a series of neutral density (ND) filters was used to attenuate the signal to achieve BER values of 10^{-9} or more. In addition to measuring beam profiles directly, the setup was simulated using a combination of an optical surface profiler and Zemax OpticStudio to obtain a better understanding of the mirrors shape and its effect on the beam profile. The mirror was first analyzed at different power levels using the profiler and then modeled in Zemax using a combination of Zernike polynomials and other terms which are defined in a later section.

3. Results

3.1. Measured Beam Profile

Using the DataRay camera, the beam profile was characterized with respect to mirror power, angle, and distance. For all measurements, the diameter is defined where the beam intensity falls to 13.5% of the peak value, also known as the $\frac{1}{e^2}$ width. As the mirror radius changes, the beam transitions from defocused, to focused, and back to defocused as shown in Figure 4. Prior to testing, the profiler was used to establish the relationship between the mirror power and the mirror's ROC. The minimum beam diameter is achieved at a power of approximately 12.9 mW which corresponds to an ROC of approximately 2.5 mm. A spherical mirror's theoretical focal length is f=(R/2), where f is the focal length and R is the radius of curvature. Therefore, if the fiber is approximated as a point source and given that the fiber is positioned 1.275 mm from the mirror, it's expected that the beam would be collimated at an ROC of 2.55 mm. This puts the measured optimal ROC within 2% of the theoretical. As the optical angle increases, the power needed for the minimum diameter along the x and y axes began to drift apart to approximately 13.1 and 12.6 mW as shown in Figure 4, which correspond to 2.54mm and 2.46mm respectively. This separation of the ROC for each axis is a product of a spherical mirror geometry. The earlier relationship between radius of curvature and focal length applies only to a spherical mirror normal to the incident beam. If there's an angle between the beam and the mirror, the focal length becomes $f_{tan} = (\frac{R}{2})\cos(\theta)$ in the tangential direction and $f_{sag} = \frac{(\frac{R}{2})}{\cos(\theta)}$ in the sagittal direction [12]. Applying these equations to the original measured data, the theoretical radius of curvature should to 2.54 mm and 2.46 mm for the x and y axis respectively, which matches the measured values.

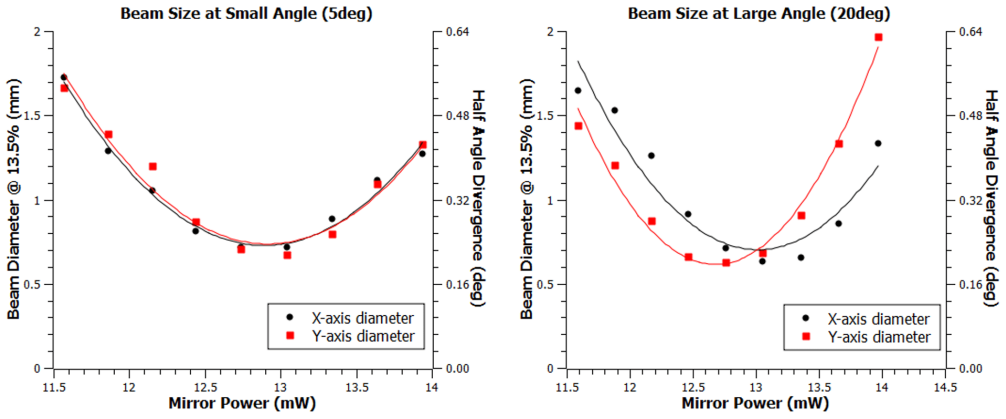

Fig. 4. Beam size versus the power to heat the mirror which corresponds to the mirrors curvature. Detector was approximately 90mm from the mirror. (left) Characterization with an optical angle of 5 degrees (right) Characterization of the beam with an optical angle of 20 degrees.

One of the advantages of this MEMS mirror is its ability to access large tilt angles. For the results in Figure 4, the optical angle was changed by manually moving the optical fiber with respect to the mirror. On the other hand, the data shown in Figure 5 was measured by titling the mirror with a bimorph. This requires that the bimorph be heated up and this extra heat affects the mirror's ROC, resulting in a larger beam size. The inconsistent beam size is a problem for many applications that demand precise control over the beam size. However, as Figure 5 shows, this

problem can be overcome by adjusting the mirror power as the bimorph actuates. This effectively compensates for the added heat and the mirror maintains the optimal curvature. When controlled correctly, the angle between the incident beam and the mirror has little effect on the reflected beams performance.

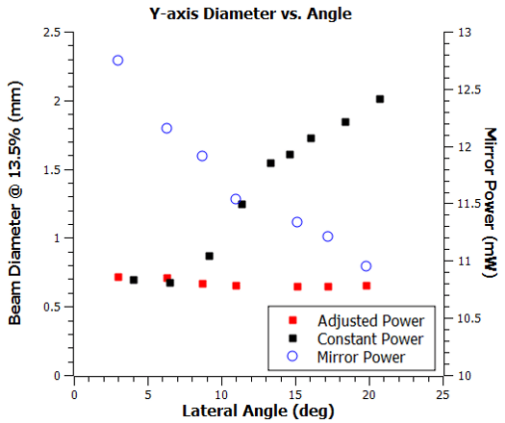

Fig. 5. The beam diameter versus angle. If the mirror power is held constant while the bimorph is actuating, the mirror's radius of curvature changes and the beam size increases. Adjusting the power at each tilt angle allows the beam size to stay relatively constant. The detector was approximately 90mm from the mirror.

One of the potential applications for this mirror is OWC, in which case the important distance range for the detector is ≤ 3 m [9, 10]. As the distance to the camera increases, the minimum beam size also increases in a linear fashion with a minimum half-angle divergence of approximately 0.18°. We believe that the reason the angle isn't smaller is because the system is approaching the diffraction limit of the mirror. At 3 m the expected beam diameter is approximately 18 mm. Figure 6 includes a comparison of the achievable beam diameters at each distance for the MEMS mirror, the optical fiber and a collimated beam as used by [9]. Since the collimated beam and optical fiber are static systems they each only have a single diameter at each distance, whereas the MEMS mirror has a range. The plot includes a measured range and a theoretical range for the mirror. The measured range includes diameters that were directly measured between 100 mm and 1,000 mm from the mirror and then extrapolated to 3,000 mm. Due to physical limitations of the camera, the beam could not be measured at the larger diameters. As shown in [8], the mirror can completely flatten and can even invert it's radius of curvature. Based on these measurements we show that the beam size has a theoretical range that continues past the measured data and then up to and slightly beyond the size of the optical fiber.

3.2. Simulated Beam Profile

To obtain a better understanding of the system, the setup was simulated using Zemax OpticStudio. The mirror was modeled using a Zernike surface as defined by Zemax, which is a combination of Zernike polynomials and other terms defined by:

$$z = \frac{cr^2}{1 + \sqrt{1 - (1 + k)c^2r^2}} + \sum_{i=1}^{8} \alpha_i r^{2i} + \sum_{i=1}^{N} A_i Z_i(\rho, \phi)$$

Where c is the curvature of the surface, k is the conic constant, the α terms are aspheric coefficients, N is the number of Zernike coefficients in the series, A_i is the coefficient for on

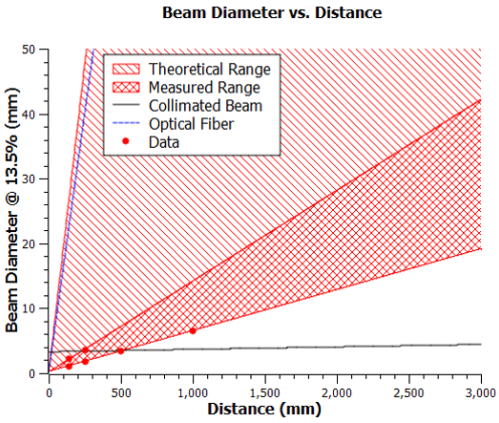

Fig. 6. Comparison between the MEMS mirror, a collimated beam (0.034° full angle [9]) and an optical fiber (9° full angle) with regards to beam diameter versus distance. The optical fiber and collimated beam have a single beam size at each distance whereas the varifocal mirror can achieve a range of sizes. The measured range is based on the measured data points.

the i^{th} Zernike polynomial, r is the radial coordinate in lens units, ρ is the normalized radial coordinate, and ϕ is the angular coordinate. During the analysis, it was determined that there was a repeated error between the scanned mirror and the modeled mirror due to curvature along the width of each mirror section. In a bimorph with a small width/length ratio, the effect of curvature in the width is small in comparison to the length. However, as shown in [13], there will also be curvature at the edges and tips which becomes more apparent at larger width/length ratio structures. In an attempt to correct for this error, a $B_1 \sin(8\phi + B_2)$ term was added to the above equation, where B_1 is a coefficient term and B_2 is angle offset. This helps compensate for some of the error between the mirror and model, and it also helps the simulated beam profile agree with the measured profile. The resulting measured and simulated profiles are shown in Figure 8 as a comparison. Figure 7 plots the results of a series of these profiles to show that the simulated beam diameters follow a similar trend to the measured data. Although there is a large spread amongst the data, there is a trend that appears and shows that the minimum diameter is roughly equivalent to the measured data. This simulation shows that although the mirror may be approximated as spherical in many regards, there are deviations from this model which may have an effect on the mirrors efficiency.

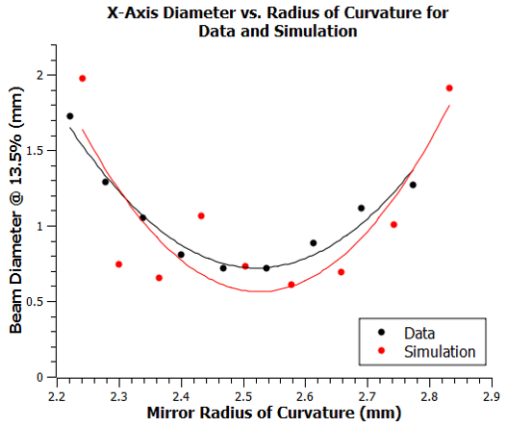

Fig. 7. Comparison of the X-axis beam diameter measured data and Zemax simulation.

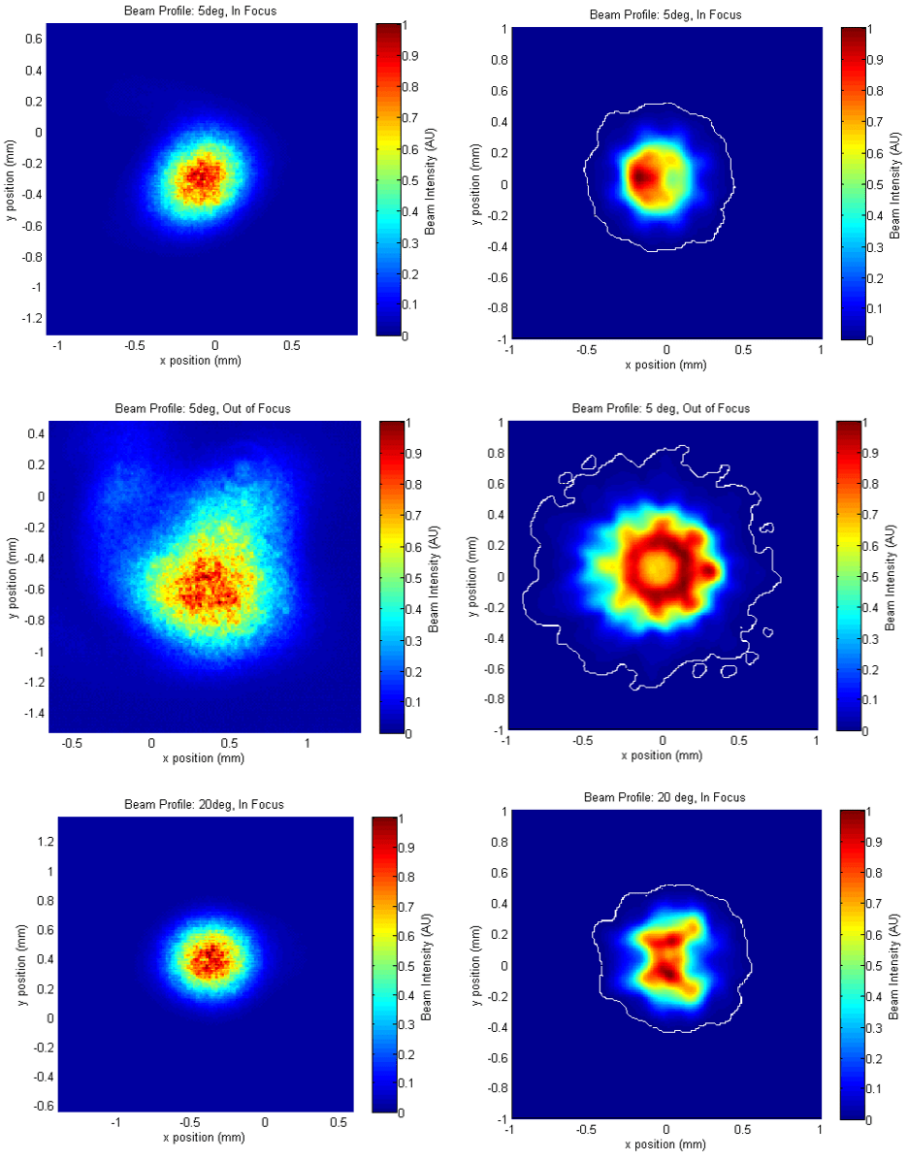

Fig. 8. Comparison of the measured and simulated beam profiles. The profiles on the left are measured profiles under difference conditions: focused at a low angle, defocused at a low angle, and focused at a larger angle. The profiles on the right are the simulated counterparts to the measured profiles.

3.3. Bit Error Rate Testing

In the application of optical communications, the BER is directly related to the SNR. For an on-off keying system with Gaussian noise, the relationship is $BER = Q(SNR)$, where Q is the complimentary error function and $SNR = (\frac{S_d}{2\sigma})$, where S_d is the difference between the 1 and 0 signal and σ^2 is the variance of the noise [14]. Focusing the beam to a smaller spot size will increase the SNR, and thus will also improve the BER of the system. Therefore, the BER was characterized with regard to the mirrors ROC, angle and distance to the detector to verify

that the mirror would improve the BER. Figure 9 compares the BER to the beam diameter and demonstrates that they both are minimized at the same mirror curvature. As the mirror curvature changes, the BER improves until it reaches the smallest spot size at which point the BER increases again. Similarly, Figure 10 shows the communication performance with respect to the mirrors angle and the detectors distance. The BER result fully agrees with the beam profile measurement, validating the model and the predicated relationship between the signal intensity and BER. As for the beam diameter, the BER increases with angle if the mirror power isn't adjusted, however it can maintain the low BER by adjusting the power at each angle. As the detector moves away and the beam size increase, the BER also increases.

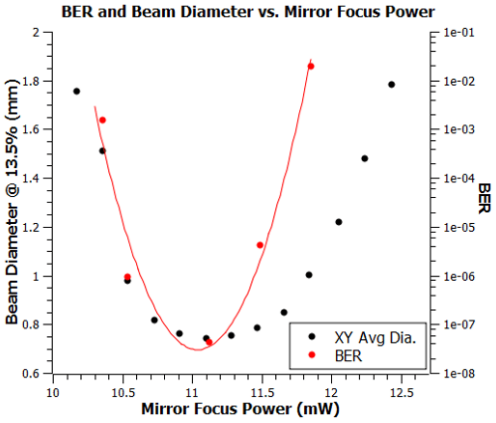

Fig. 9. Comparison of the beam diameter and the BER relative to the mirror power. This shows that as the beam diameter decreases the BER also decreases. Using the mirror to focus the beam to a smaller spot size significantly improves the BER. Detector was approximately 90 mm from the mirror.

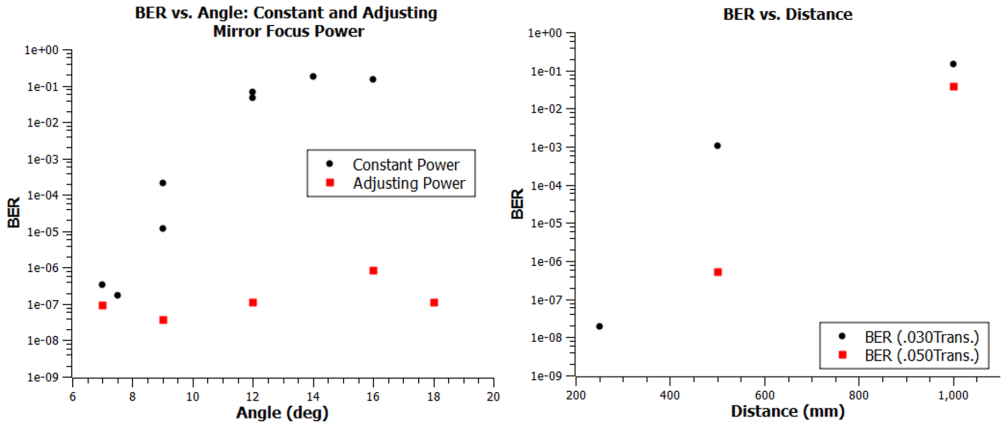

Fig. 10. Similar results to the beam diameter confirm that the BER closely follows the trend of the beam diameter. (left) BER versus the mirror angle shows that if the power is not adjusted the BER will deteriorate, whereas adjusting the power to maintain a focused beam the BER can stay relatively constant. The detector was approximately 130 mm from the mirror. (right) As the detector gets further from the mirror the error rate increases. This plot includes data using two different filter setups. The black circles are data using a filter that allowed 3% of the light to be transmitted and the red squares used a filter that allowed 5% of the light to be transmitted.

In a communication system where the detector's location can move such as a phone or a laptop, it's important to have a device that can steer a beam and Figure 11 highlights why. In contrast to the rest of the experiments, this test used a stationary detector and the beam was swept across it as shown in Figure 10. When the beam is on center, the BER is at its minimum. Similar to [10], we find that as the beam moves off center in either direction, the BER increases. The ability to place the beam on the center of the detector has a significant impact on the signal strength and the BER. When aligned and focused we obtain error free transmission.

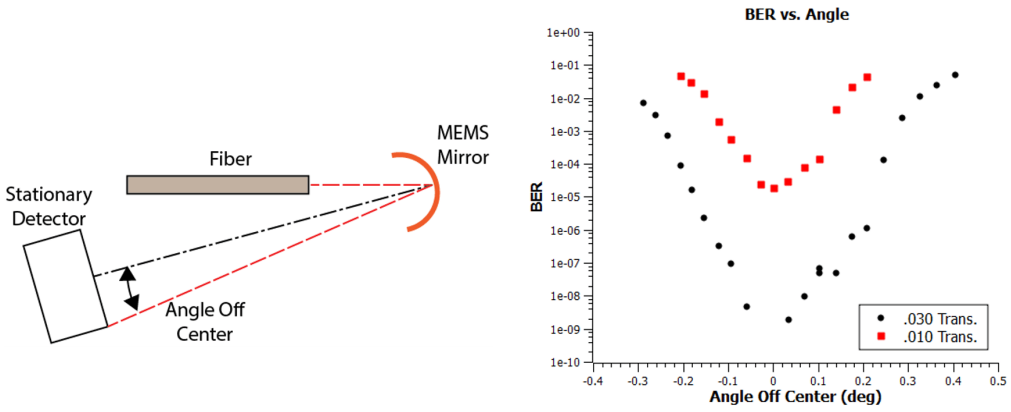

Fig. 11. (left) Illustration (not to scale) of setup used to test the effect of sweeping a beam across a stationary detector on the BER (right) BER as the beam moves away from the center of the detector. This plot includes data using two different filter setups. The black circles are data using a filter that allowed 3% of the light to be transmitted and the red squares used a filter that allowed 1% of the light to be transmitted. Detector was approximately 250 mm from the mirror.

4. Conclusion

This paper characterizes the beam shaping and communication performance of a large focal range MEMS mirror. This focal range combined with the large tip-tilt angle provides this device with a unique level of dynamic control with regard to both beam steering and shaping which allows it to tune the light in-situ. This micromirror may be approximated as spherical with regard to many optical properties and is capable of focusing light to a beam with a .18° half-angle divergence. Thus, at a distance of 3 m the mirror can focus the fiberized beam to an 18 mm diameter spot. In order to make significant improvements on the beam size would require a change in mirror geometry as this performance is approaching the diffraction of the mirror. The ability to change the shape of fiberized light from a wide to a narrow beam provides dynamic tunability to systems such as optical communications.

Funding

This work was supported primarily by the Engineering Research Centers Program of the National Science Foundation under NSF Cooperative Agreement No. EEC-0812056. Any opinions, findings and conclusions or recommendations expressed in this material are those of the author(s) and do not necessarily reflect those of the National Science Foundation.